


Readout-Induced Suppression and Enhancement of Superconducting Qubit LifetimesTed Thorbeck^{1,*}, Zhihao Xiao², Archana Kamal,² and Luke C. G. Govia³¹*IBM Quantum, IBM T. J. Watson Research Center, Yorktown Heights, New York 10598, USA*²*Department of Physics and Applied Physics, University of Massachusetts, Lowell, Massachusetts 01854, USA*³*IBM Quantum, IBM Almaden Research Center, San Jose, California 95120, USA* (Received 12 September 2023; accepted 23 January 2024; published 29 February 2024)

It has long been known that the lifetimes of superconducting qubits suffer during readout, increasing readout errors. We show that this degradation is due to the anti-Zeno effect, as readout-induced dephasing broadens the qubit so that it overlaps “hot spots” of strong dissipation, likely due to two-level systems in the qubit’s bath. Using a flux-tunable qubit to probe the qubit’s frequency-dependent loss, we accurately predict the change in lifetime during readout with a new self-consistent master equation that incorporates the modification to qubit relaxation due to measurement-induced dephasing. Moreover, we controllably demonstrate both the Zeno and anti-Zeno effects, which can explain both suppression and the rarer enhancement of qubit lifetimes during readout.

DOI: [10.1103/PhysRevLett.132.090602](https://doi.org/10.1103/PhysRevLett.132.090602)

Introduction.—The speed and simplicity of dispersive readout has made it the dominant readout technique for superconducting qubits, despite long-standing mysteries about why dispersive readout sometimes changes the qubit state [1–3]. These are called non-quantum-nondemolition (non-QND) errors, to distinguish them from the trivial errors that occur when the measurement tone is too weak, or too much readout signal is lost, and there is not enough information to distinguish the qubit states. Readout errors threaten quantum computing because they add to the overhead for long-term goals like quantum error correction or near-term applications such as error mitigation [4–7]. They also frustrate dynamic circuits, in which operations are conditioned on the outcome of midcircuit measurements [8].

Relaxation and leakage are the two dominant non-QND errors of superconducting qubit readout. Recent work has shown that readout-induced leakage, i.e., occupying a state outside the qubit subspace, can occur when a transition frequency from the qubit subspace to a highly excited state is resonant with an occupied resonator state, allowing excitations to swap into the transmon [9–15]. Because the qubit has a finite lifetime T_1 , relaxation errors are expected during readout, but T_1 is often suppressed during readout, resulting in an excess of readout errors. However, T_1 sometimes increases during readout, or T_1 can be a nonmonotonic function of readout strength [16–21]. Early work showed that backaction from the measurement apparatus could degrade T_1 , but this has been mitigated by adding isolation between the readout resonator and the amplifier [21–23]. Another possible explanation is dressed dephasing [24–26], in which photons in the resonator combine with dephasing noise at the detuning frequency between the qubit and the readout resonator, causing

excitation or relaxation in the qubit. However, this can be minimized by protecting the qubit from dephasing noise at the detuning frequency.

Much of the recent theoretical work on T_1 suppression during readout has focused on how the readout drive changes the Purcell loss, i.e., qubit dissipation due to its coupling to the lossy readout resonator [27–33]. As the strength of the measurement tone changes the qubit-resonator hybridization, it also changes the Purcell loss. While initial models predicted an increase in T_1 , more recent work predicts a decrease in T_1 is possible, which qualitatively agrees with experiment. However Purcell loss is typically engineered to be very small via a Purcell filter [34,35], so increasing it is unlikely to be the origin of excess relaxation. Therefore, the dominant cause of the suppression of T_1 during readout is still a mystery, and solving it will not only help us engineer protection into quantum processors, but also answer a long-standing, unresolved question in the field of open quantum systems.

In this Letter, we show that the change in the lifetime of superconducting qubits during readout is due to the quantum Zeno and anti-Zeno effects. The quantum Zeno effect predicts that measurement should freeze a quantum system, resulting in nonexponential behavior and preventing radiative decay and increasing the system’s lifetime [36,37]. The initial work on the quantum Zeno effect was based on very general arguments; however, as the details of realistic quantum systems were considered, such as the spectrum of the environment, it was discovered that the opposite effect, i.e., measurement increasing the rate of decay, called the anti-Zeno effect, is far more common [38–40]. The Zeno effect has been experimentally demonstrated in superconducting qubits [16,41,42], and it has been used for qubit control [43] and gates [44], but it has not been

invoked to explain the change in T_1 during readout of superconducting qubits.

We begin by reinterpreting the anti-Zeno effect in terms familiar to the circuit-QED community: during readout, the qubit's transition is both broadened by dephasing and Stark shifted. The transmon is coupled to a dissipative bath, whose spectrum typically has some structure as a function of frequency. T_1 is typically reduced during readout because the broadened qubit is more likely to interact with hot spots of higher dissipation. We believe that in our device two-level systems (TLSs) are the dominant source of hot spots, but any parasitic device or package modes would induce similar behavior. In contrast, the lifetime of the qubit would not change during readout for a transmon with a uniform spectrum. While it has previously been suggested that readout can be degraded if the qubit is Stark shifted into a TLS [9,20], we show that it is dephasing, not Stark shift, that is essential to understanding the suppression of qubit lifetimes during readout. We also show that this is the dominant explanation for the change in qubit lifetime during readout in a modern superconducting quantum processor, by using a flux-tunable qubit to map the qubit's decay rate as a function of frequency, which we use to predict how T_1 changes during readout. While the Zeno and anti-Zeno effects are well known, modeling these effects challenges the traditional Lindbladian master equation approach for dissipation in superconducting circuits because the qubit interacts with two baths, one for dephasing and the other for dissipative decay. During readout, the interaction with the dephasing bath is much stronger than the interaction with the dissipative bath, so our model needs to capture how the first bath influences the system-bath interaction of the second. Using the methodology of Ref. [45], we show how to self-consistently address the impact of dephasing on the qubit's coupling to the dissipative bath and extend the Kofman-Kurizki formula for the Zeno and anti-Zeno effect to encompass coherent couplings to an ancilla system [38–40].

Anti-Zeno effect and T_1 during readout.—From qubit lifetime spectroscopy, measuring T_1 as a function of the qubit frequency, it is well known that $\gamma_q = 1/T_1$ is not a constant; there are hot spots, likely due to TLS or packaging modes, where the decay rate is higher [Fig. 1(a)] [46–50]. To understand how the qubit lifetime changes during measurement, we neglect the dynamics of the readout resonator to focus only on how the measurement affects the qubit. First, during readout, the qubit frequency is Stark shifted, leading to a detuning from its natural frequency by $\nu_S = 2\chi\bar{n}_r$, where χ is the dispersive shift and \bar{n}_r is the average number of photons in the readout resonator. Second, measurement destroys the qubit's coherence, i.e., it dephases the qubit, as described by an exponential decay rate $\gamma_\phi(\bar{n}_r)$. Dephasing can be understood as uncertainty in the qubit's frequency, so during readout we need to consider all possible qubit frequencies instead of solely

considering the natural qubit frequency. As derived in Refs. [45,51], the Kofman-Kurizki formula [38–40] relates the qubit decay rate during continuous measurement,

$$\Gamma(\bar{n}_r) = \int_{-\infty}^{\infty} \gamma_q(\omega) \frac{1}{\pi} \frac{\gamma_\phi(\bar{n}_r)}{\gamma_\phi(\bar{n}_r)^2 + (\omega - \tilde{\omega}_q(\bar{n}_r))^2} d\omega, \quad (1)$$

to an integral that computes the average of the qubit's decay rate over frequency weighted by a Lorentzian centered on the Stark-shifted qubit frequency, $\tilde{\omega}_q(\bar{n}_r) = \omega_q + \nu_S$, with a width equal to the dephasing rate. This Lorentzian is similar to the qubit absorption spectrum during readout derived in [51,56]. As the measurement strength goes to zero, $\bar{n}_r, \nu_S, \gamma_\phi \rightarrow 0$, the Lorentzian approaches a δ function, so the decay rate reduces to that given by Fermi's golden rule at the natural qubit frequency, $\Gamma \rightarrow \gamma_q(\omega_q)$ [51]. In the case where the qubit's decay rate γ_q is uniform as a function of frequency, then the lifetime of the qubit does not change during readout.

The key insight from the anti-Zeno effect literature is that evaluating the Kofman-Kurizki formula is more likely to result in the anti-Zeno effect than the Zeno effect [38–40]. Consider a typical plot of $\gamma_q(\omega)$, Fig. 1(a). The Lorentzian shows that, as readout strength is increased, the qubit is Stark shifted to lower frequencies and broadened by the dephasing, until the Lorentzian overlaps a hot spot. As shown in Fig. 1(c), the Kofman-Kurizki formula predicts an increase in the decay rate: the anti-Zeno effect. The Zeno effect can be observed when the natural qubit frequency is aligned with a hot spot, so that measurement moves the qubit to a region of slower decay, Fig. 1(b). Because the qubit is not typically resonant with a hot spot, the anti-Zeno effect is more common than the Zeno effect.

To test this theory, we compare the measured qubit decay rate during readout to the Kofman-Kurizki prediction. To

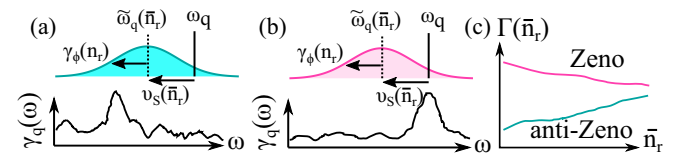


FIG. 1. Fundamentals of Zeno and anti-Zeno effects. (a) The qubit decay rate in the absence of readout $\gamma_q(\omega)$ is dominated by a few hot spots, likely due to TLSs. During readout the qubit's frequency is Stark shifted by $\nu_S(\bar{n}_r)$ and broadened at the dephasing rate $\gamma_\phi(\bar{n}_r)$, as shown by the Lorentzian centered about the Stark-shifted qubit frequency $\tilde{\omega}_q(\bar{n}_r)$. Here the Lorentzian overlaps a hot spot that the qubit is not sensitive to at its natural frequency, thus increasing the decay rate. (b) To display the Zeno effect, the natural qubit frequency must be resonant with a hot spot, so that during readout the qubit becomes less sensitive to the hot spot. (c) Schematic of how the decay rate during readout $\Gamma(\bar{n}_r)$ depends on the readout strength, in terms of the average number of photons in the resonator, for both the Zeno and anti-Zeno effects.

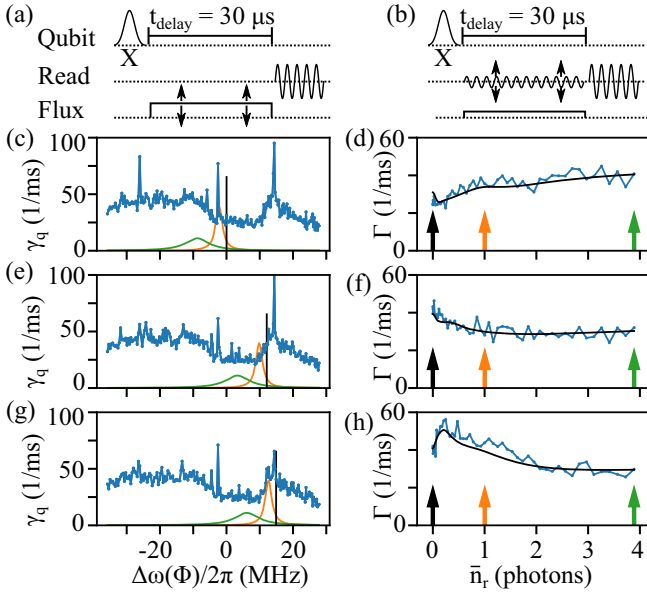


FIG. 2. Predicting $\Gamma(\bar{n}_r)$ using the Kofman-Kurizki formula. (a) Fixed-delay T_1 experiment, with $t_{\text{delay}} = 30 \mu\text{s}$, to measure the qubit decay rate $\gamma_q(\omega)$ using flux to shift the qubit frequency by $\Delta\omega(\Phi)$ about the natural qubit frequency, $\omega_q/2\pi = 4.884 \text{ GHz}$. We convert qubit population at the end of the experiment p_1 to a decay rate using $\gamma_q = -\log(p_1)/t_{\text{delay}}$, neglecting heating and imperfect initialization. (b) Fixed-delay T_1 experiment with a pseudomeasurement pulse, of strength \bar{n}_r , during the delay to measure the decay rate during readout $\Gamma(\bar{n}_r)$. (a),(b) Interleaved into a single experiment, lasting about 100 s, to prevent drift in $\gamma_q(\omega)$. (c),(e),(g) Results of $\gamma_q(\omega)$ sweep in blue. (d),(f),(h) Experimental results of $\Gamma(\bar{n}_r)$ sweep in blue, with the Kofman-Kurizki prediction in black. A flux offset applied during pseudomeasurement tone shifts the portion of $\gamma_q(\omega)$ that is sampled during readout, to switch between the Zeno and anti-Zeno effects. The vertical black line on the left shows the flux-tuned qubit frequency at $\bar{n}_r = 0$, black arrow on right. The colored Lorentzians show the portions of $\gamma_q(\omega)$ involved in evaluating the Kofman-Kurizki formula at $\bar{n}_r \approx 1$ and $\bar{n}_r \approx 4$, as shown by the colored arrows on the right.

measure $\gamma_q(\omega)$, we used a flux pulse to tune the qubit frequency during a fixed-delay T_1 experiment, Fig. 2(a). Then we measured the decay rate during readout $\Gamma(\bar{n}_r)$ as a function of readout power, Fig. 2(b). The blue traces in Figs. 2(c) and 2(d) show the results of these two measurements. Figure 2(d) shows $\Gamma(\bar{n}_r)$ increasing with readout power: the anti-Zeno regime. A numerical evaluation of the Kofman-Kurizki formula, black line in Fig. 2(d), successfully predicts the measured $\Gamma(\bar{n}_r)$. We can understand this prediction by looking at Fig. 2(c). The natural qubit frequency, black line in Fig. 2(c) and black arrow in Fig. 2(d), is not aligned with any hot spots. As shown by the orange and green Lorentzians in Fig. 2(c), corresponding to the orange and green arrows in Fig. 2(d), the qubit becomes sensitive to a region with a higher qubit

decay rate as the readout power increases. Thus, the qubit experiences a higher decay during readout.

Flux tuning the qubit toward a hot spot changes the behavior from anti-Zeno to Zeno in a predictable manner. In Fig. 2(c) there is a broad peak in the decay rate above the natural qubit frequency. To study this peak, we add a flux pulse during the pseudomeasurement tone to position the qubit on the left shoulder of the peak during the measurement of $\Gamma(\bar{n}_r)$ as shown in Figs. 2(e) and 2(f). Figure 2(e) shows that the Stark shift and dephasing bring the qubit away from the peak and into a valley where the qubit decay rate is slower, which manifests in Fig. 2(f) as the decay rate decreasing with increasing readout strength, i.e., the Zeno effect. Next, in Figs. 2(g) and 2(h), we situate the qubit just to the right of the peak. In Fig. 2(h), $\Gamma(\bar{n}_r)$ is nonmonotonic, at first increasing and then decreasing. We interpret this in Fig. 2(g) as the readout at first bringing the qubit to the peak and then past it. Thus, the Kofman-Kurizki formula accurately quantifies the change in qubit T_1 observed during measurement in both the Zeno and anti-Zeno regimes. In the Supplemental Material [51], we show that changes in the $\gamma_q(\omega)$ over time are correlated with changes in $\Gamma(\bar{n}_r)$, which can only be explained by the anti-Zeno effect.

Breakdown of Kofman-Kurizki formula.—We have used the Kofman-Kurizki formula to predict the behavior of T_1 during readout; however, Fig. 3 shows the Kofman-Kurizki formula failing to predict the measured $\Gamma(\bar{n}_r)$ when a TLS coherently couples to the qubit. The experimental conditions in Fig. 3 are identical to those in Fig. 2, with the only change to the setup being the uncontrollable emergence of a TLS at $\Delta\omega(\Phi)/2\pi = -11 \text{ MHz}$, perhaps due to

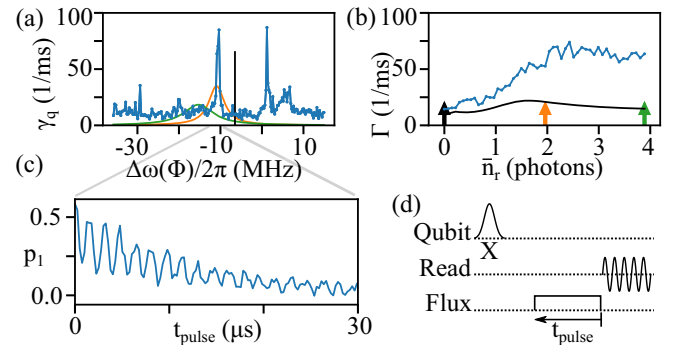


FIG. 3. Breakdown of the Kofman-Kurizki prediction. (a),(b) Repetition of the experiment from Fig. 2, taken about a month later, showing the failure of the Kofman-Kurizki formula to predict the measured $\Gamma(\bar{n}_r)$. Here the orange Lorentzian shows the dephasing broadened range of the qubit when the Stark shift is approximately equal to the detuning to the TLS, at about $\bar{n}_r \approx 2$. (c) Qubit p_1 during swap spectroscopy, showing oscillations between the qubit and the TLS. (d) Swap spectroscopy for the TLS at $\Delta/2\pi = -11 \text{ MHz}$ in (a). Delay between the X pulse and the measurement tone was fixed at $50 \mu\text{s}$, so p_1 does not approach unity at $t_{\text{pulse}} = 0$ in (c).

the impact of radiation [57]. This clearly shows that changes in $\gamma_q(\omega)$ cause the change in $\Gamma(\bar{n}_r)$. The data in Fig. 3(b) also clearly show that the Stark shift alone cannot explain our results, given the absence of a narrow peak when the Stark shift equals the qubit-TLS detuning.

To understand why the Kofman-Kurizki formula significantly underestimates the measured $\Gamma(\bar{n}_r)$ in Fig. 3(b), we used swap spectroscopy to look at the TLS, Figs. 3(c) and 3(d). This shows vacuum-Rabi oscillations between the qubit and the TLS. After $t_{\text{pulse}} = 30 \mu\text{s}$ [used in Figs. 3(a) and 3(b)], the population is still oscillating, so fitting a single exponential is inappropriate. This is an example of a strongly coupled TLS, in which the coupling strength g is larger than the decoherence rates, both relaxation or dephasing, for both the qubit and the TLS, but not the measurement-induced dephasing. Moreover, the derivation of the Kofman-Kurizki formula makes the Markov assumption, that once the qubit decays to the bath, the excitation cannot return [38,45,51,58]. The vacuum-Rabi oscillations in Fig. 3(c) demonstrate that the Markov approximation, and thus the Kofman-Kurizki formula, is no longer valid, likely because the qubit-TLS interaction is stronger than the bath equilibration rate (TLS intrinsic dissipation).

Artificial TLS.—Given their uncontrollable dynamics, studying a natural TLS is challenging, so instead we manufacture a coherent TLS, called the “defect,” by engineering a transmon with strong coupling to off-chip dissipation to have a very short lifetime, $\gamma_{1,D} = 1/(103 \text{ ns})$. It is coupled to the first transmon with strength $g_D/2\pi = 1.6 \text{ MHz}$ [51]. The defect is a quantum object, with its own bath, through which the qubit can decay via an effect analogous to Purcell decay. Our goal is to understand how qubit measurement impacts the decay of the qubit through the defect.

Flux tuning the qubit such that it is near resonant with the defect at $\omega_D/2\pi \approx 4.3 \text{ GHz}$ brings it into a regime where it is very sensitive to flux noise. Thus, rather than using a pseudomeasurement tone, we add flux noise to obtain enhanced qubit dephasing without a Stark shift. As demonstrated in Refs. [16,59], pure dephasing is a “quasimeasurement” that can cause the Zeno and anti-Zeno effects. One can also interpret our construction of the Kofman-Kurizki formula as highlighting the fact that dephasing is the necessary ingredient for the Zeno and anti-Zeno effects, and the role of measurement is to supply that dephasing, demonstrating that it, not the Stark shift, is essential to explain changes in T_1 during readout.

Figure 4(c) shows the measured Γ of the qubit as a function of qubit-defect detuning and flux-noise-induced dephasing rate. For large detuning and small amounts of flux noise, $\Gamma \approx 1/100 \mu\text{s}$ is limited by the background T_1 of the qubit. As the qubit comes into resonance with the defect, Γ increases by 3 orders of magnitude. Line cuts through Fig. 4(c), shown in Fig. 4(b), demonstrate that our intuition for the regimes of the Zeno and anti-Zeno effects

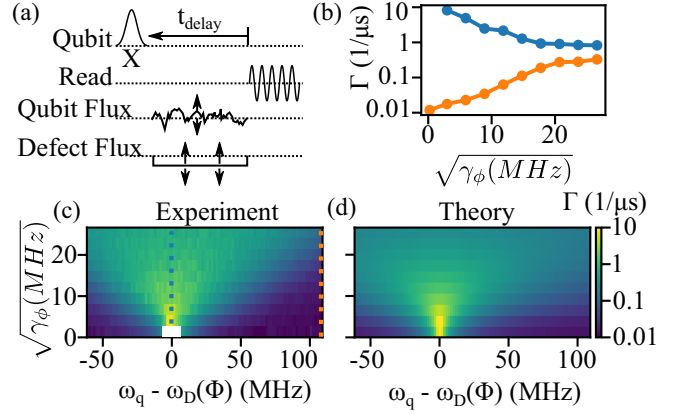


FIG. 4. Zeno and anti-Zeno effects for a qubit coupled to a coherent defect. (a) Variable-delay T_1 experiment, with logarithmic spacing to fit Γ over orders of magnitude, as a function of both the magnitude of the flux noise applied to the qubit and the qubit-defect detuning. The qubit frequency is fixed at $\omega_q/2\pi = 4.291 \text{ GHz}$, while the flux through the defect is swept. (b) Two line cuts through (c): blue for qubit on resonance with the defect, showing the Zeno effect, and orange for the qubit far from resonance with the defect, showing the anti-Zeno effect. (c) Measured Γ as a function of dephasing rate and qubit-defect detuning. Points near zero detuning and zero applied flux noise are not shown because vacuum-Rabi oscillations do not fit a simple exponential. (d) Theory prediction of Γ using Eq. (2) and parameters independently measured in the Supplemental Material [51].

applies even for a strongly coupled coherent defect [60]. Near the defect, adding dephasing noise decreases the decay rate (the Zeno effect), while away from the defect, adding noise increases the decay rate (the anti-Zeno effect). In this regime, we need an extension of the Kofman-Kurizki formula for a qubit coupled to a coherent TLS. To do this, we no longer treat the TLS as part of the bath; instead, it is treated as an auxiliary quantum system that is coupled to the qubit and which has strong intrinsic dissipation. This allows us to adiabatically eliminate the defect TLS, and our elimination technique developed in Refs. [45,51] allows us to include the dephasing on the qubit into the calculation of the decay rate of the qubit into the defect’s bath. To do this, in Refs. [45,51] we model the defect transmon as a harmonic oscillator and we use adiabatic elimination to remove the defect and calculate the decay rate of the qubit into the defect’s bath in the presence of dephasing on the qubit. The total decay rate of the qubit Γ is then

$$\Gamma = \gamma_q + 2g_D^2 \frac{\gamma_\phi + \gamma_{1,D}/2 - \gamma_q/2}{(\gamma_\phi + \gamma_{1,D}/2 - \gamma_q/2)^2 + (\omega_q - \omega_D)^2}. \quad (2)$$

By ignoring the loss (γ_q) and dephasing (γ_ϕ) in the qubit, we recover the standard formula for Purcell loss, so our expression is a generalization of Purcell loss that accounts for dephasing [61]. In Fig. 4(d), we plot Γ , showing excellent agreement with the experiment. All the parameters

are independently measured in the Supplemental Material [51]; there are no fitting parameters.

Conclusion.—We have shown that the quantum Zeno and anti-Zeno effects are the dominant cause of the suppression and enhancement of decay during readout for a modern superconducting qubit. We have successfully predicted change in decay rates during readout by accounting for how the measurement-induced Stark shift and dephasing change the qubit’s interaction with its radiative bath. This is a fundamental open system effect, because, while a flux pulse can be used to counteract the Stark shift, the dephasing-induced broadening of the qubit is intrinsic to measurement. We switch between the Zeno and anti-Zeno effects by changing the portion of $\gamma_q(\omega)$ that is sampled during readout, which can be used to minimize the degradation of T_1 during readout. Qubit tunability is routinely used to optimize the lifetime of the qubit [46,47,49], but to maximize T_1 during readout to ensure truly QND readout, the optimization should consider the dephasing-broadened range of qubit frequencies. Moreover, the anti-Zeno effect is an example of two decoherence mechanisms interacting; i.e., readout-induced dephasing changing the radiative dissipation. Our work represents experimental validation of the methodology of the self-consistent master equation [45], lending confidence that similar problems can be understood and mitigated in other quantum systems using this technique.

We thank Hannah Varekamp, Moein Malekakhlagh, Sami Rosenblatt, Hasan Nayfeh, Dave McKay, Muir Kumph, and Juzar Thinga for helpful conversations. T. T. and L. G. were supported by the Army Research Office under QCISS (Contract No. W911NF-21-1-0002) and device characterization by IARPA under LogiQ (W911NF-16-1-0114). Z. X. and A. K. were supported by Air Force Office of Scientific Research (AFOSR) under Grant No. FA9550-21-1-0151 and NSF under Grant No. DMR-2047357. The device used in this work was designed and fabricated internally at IBM Quantum.

The views and conclusions contained in this document are those of the authors and should not be interpreted as representing the official policies, either expressed or implied, of the Army Research Office, IARPA, or the U.S. Government. The U.S. Government is authorized to reproduce and distribute reprints for Government purposes notwithstanding any copyright notation herein.

* ted.thorbeck@ibm.com

- [1] A. Blais, R.-S. Huang, A. Wallraff, S. M. Girvin, and R. J. Schoelkopf, *Phys. Rev. A* **69**, 062320 (2004).
 [2] A. Blais, A. L. Grimsmo, S. M. Girvin, and A. Wallraff, *Rev. Mod. Phys.* **93**, 025005 (2021).

- [3] A. Wallraff, D. I. Schuster, A. Blais, L. Frunzio, J. Majer, M. H. Devoret, S. M. Girvin, and R. J. Schoelkopf, *Phys. Rev. Lett.* **95**, 060501 (2005).
 [4] S. Bravyi, S. Sheldon, A. Kandala, D. C. McKay, and J. M. Gambetta, *Phys. Rev. A* **103**, 042605 (2021).
 [5] E. van den Berg, Z. K. Mineev, and K. Temme, *Phys. Rev. A* **105**, 032620 (2022).
 [6] A. G. Fowler, M. Mariantoni, J. M. Martinis, and A. N. Cleland, *Phys. Rev. A* **86**, 032324 (2012).
 [7] F. Leymann and J. Barzen, *Quantum Sci. Technol.* **5**, 044007 (2020).
 [8] A. D. Córcoles, M. Takita, K. Inoue, S. Lekuch, Z. K. Mineev, J. M. Chow, and J. M. Gambetta, *Phys. Rev. Lett.* **127**, 100501 (2021).
 [9] D. Sank, Z. Chen, M. Khezri, J. Kelly, R. Barends, B. Campbell, Y. Chen, B. Chiaro, A. Dunsworth, A. Fowler *et al.*, *Phys. Rev. Lett.* **117**, 190503 (2016).
 [10] M. Khezri, A. Opremcak, Z. Chen, A. Bengtsson, T. White, O. Naaman, R. Acharya, K. Anderson, M. Ansmann, F. Arute *et al.*, *Phys. Rev. Appl.* **20**, 054008 (2023).
 [11] R. Shillito, A. Petrescu, J. Cohen, J. Beall, M. Hauru, M. Ganahl, A. G. M. Lewis, G. Vidal, and A. Blais, *Phys. Rev. Appl.* **18**, 034031 (2022).
 [12] J. Cohen, A. Petrescu, R. Shillito, and A. Blais, *PRX Quantum* **4**, 020312 (2023).
 [13] L. Verney, R. Lescanne, M. H. Devoret, Z. Leghtas, and M. Mirrahimi, *Phys. Rev. Appl.* **11**, 024003 (2019).
 [14] R. Lescanne, L. Verney, Q. Ficheux, M. H. Devoret, B. Huard, M. Mirrahimi, and Z. Leghtas, *Phys. Rev. Appl.* **11**, 014030 (2019).
 [15] M. Malekakhlagh, W. Shanks, and H. Paik, *Phys. Rev. A* **105**, 022607 (2022).
 [16] P. M. Harrington, J. T. Monroe, and K. W. Murch, *Phys. Rev. Lett.* **118**, 240401 (2017).
 [17] J. E. Johnson, C. Macklin, D. H. Slichter, R. Vijay, E. B. Weingarten, J. Clarke, and I. Siddiqi, *Phys. Rev. Lett.* **109**, 050506 (2012).
 [18] Z. K. Mineev, S. O. Mundhada, S. Shankar, P. Reinhold, R. Gutiérrez-Jáuregui, R. J. Schoelkopf, M. Mirrahimi, H. J. Carmichael, and M. H. Devoret, *Nature (London)* **570**, 200 (2019).
 [19] D. Gusenkova, M. Spiecker, R. Gebauer, M. Willsch, D. Willsch, F. Valenti, N. Karcher, L. Grünhaupt, I. Takmakov, P. Winkel *et al.*, *Phys. Rev. Appl.* **15**, 064030 (2021).
 [20] V. Sivak, A. Eickbusch, B. Royer, S. Singh, I. Tsioutsios, S. Ganjam, A. Miano, B. Brock, A. Ding, L. Frunzio *et al.*, *Nature (London)* **616**, 50 (2023).
 [21] F. Mallet, F. R. Ong, A. Palacios-Laloy, F. Nguyen, P. Bertet, D. Vion, and D. Esteve, *Nat. Phys.* **5**, 791 (2009).
 [22] T. Picot, A. Lupaşcu, S. Saito, C. J. P. M. Harmans, and J. E. Mooij, *Phys. Rev. B* **78**, 132508 (2008).
 [23] I. Serban, M. I. Dykman, and F. K. Wilhelm, *Phys. Rev. A* **81**, 022305 (2010).
 [24] M. Boissonneault, J. M. Gambetta, and A. Blais, *Phys. Rev. A* **77**, 060305(R) (2008).
 [25] M. Boissonneault, J. M. Gambetta, and A. Blais, *Phys. Rev. A* **79**, 013819 (2009).
 [26] D. H. Slichter, R. Vijay, S. J. Weber, S. Boutin, M. Boissonneault, J. M. Gambetta, A. Blais, and I. Siddiqi, *Phys. Rev. Lett.* **109**, 153601 (2012).

- [27] E. A. Sete, J. M. Gambetta, and A. N. Korotkov, *Phys. Rev. B* **89**, 104516 (2014).
- [28] M. Malekakhlagh, A. Petrescu, and H. E. Türeci, *Phys. Rev. B* **101**, 134509 (2020).
- [29] A. Petrescu, M. Malekakhlagh, and H. E. Türeci, *Phys. Rev. B* **101**, 134510 (2020).
- [30] R. Hanai, A. McDonald, and A. Clerk, *Phys. Rev. Res.* **3**, 043228 (2021).
- [31] M. Boissonneault, J. M. Gambetta, and A. Blais, *Phys. Rev. Lett.* **105**, 100504 (2010).
- [32] E. A. Sete, J. M. Martinis, and A. N. Korotkov, *Phys. Rev. A* **92**, 012325 (2015).
- [33] C. Müller, *Phys. Rev. Res.* **2**, 033046 (2020).
- [34] M. D. Reed, B. R. Johnson, A. A. Houck, L. DiCarlo, J. M. Chow, D. I. Schuster, L. Frunzio, and R. J. Schoelkopf, *Appl. Phys. Lett.* **96**, 203110 (2010).
- [35] E. Jeffrey, D. Sank, J. Y. Mutus, T. C. White, J. Kelly, R. Barends, Y. Chen, Z. Chen, B. Chiaro, A. Dunsworth *et al.*, *Phys. Rev. Lett.* **112**, 190504 (2014).
- [36] B. Misra and E. G. Sudarshan, *J. Math. Phys. (N.Y.)* **18**, 756 (1977).
- [37] W. M. Itano, D. J. Heinzen, J. J. Bollinger, and D. J. Wineland, *Phys. Rev. A* **41**, 2295 (1990).
- [38] A. G. Kofman and G. Kurizki, *Nature (London)* **405**, 546 (2000).
- [39] A. Kofman and G. Kurizki, *Z. Naturforsch. A* **56**, 83 (2001).
- [40] A. G. Kofman, G. Kurizki, and T. Opatrny, *Phys. Rev. A* **63**, 042108 (2001).
- [41] K. Kakuyanagi, T. Baba, Y. Matsuzaki, H. Nakano, S. Saito, and K. Semba, *New J. Phys.* **17**, 063035 (2015).
- [42] D. Slichter, C. Müller, R. Vijay, S. Weber, A. Blais, and I. Siddiqi, *New J. Phys.* **18**, 053031 (2016).
- [43] S. Hacohe-Gourgy, L. P. García-Pintos, L. S. Martin, J. Dressel, and I. Siddiqi, *Phys. Rev. Lett.* **120**, 020505 (2018).
- [44] E. Blumenthal, C. Mor, A. A. Diringer, L. S. Martin, P. Lewalle, D. Burgarth, K. B. Whaley, and S. Hacohe-Gourgy, *npj Quantum Inf.* **8**, 88 (2022).
- [45] Z. Xiao, J. Thinga, T. Thorbeck, L. C. G. Govia, and A. Kamal (to be published).
- [46] P. V. Klimov, J. Kelly, Z. Chen, M. Neeley, A. Megrant, B. Burkett, R. Barends, K. Arya, B. Chiaro, Y. Chen *et al.*, *Phys. Rev. Lett.* **121**, 090502 (2018).
- [47] M. Carroll, S. Rosenblatt, P. Jurcevic, I. Lauer, and A. Kandala, *npj Quantum Inf.* **8**, 132 (2022).
- [48] R. Barends, J. Kelly, A. Megrant, D. Sank, E. Jeffrey, Y. Chen, Y. Yin, B. Chiaro, J. Mutus, C. Neill *et al.*, *Phys. Rev. Lett.* **111**, 080502 (2013).
- [49] J. Lisenfeld, A. Bilmes, and A. V. Ustinov, *npj Quantum Inf.* **9**, 8 (2023).
- [50] C. Müller, J. H. Cole, and J. Lisenfeld, *Rep. Prog. Phys.* **82**, 124501 (2019).
- [51] See Supplemental Material at <http://link.aps.org/supplemental/10.1103/PhysRevLett.132.090602> for calibration details, additional data, and full derivations, which includes Refs. [52–55].
- [52] A. A. Clerk, M. H. Devoret, S. M. Girvin, F. Marquardt, and R. J. Schoelkopf, *Rev. Mod. Phys.* **82**, 1155 (2010).
- [53] S. M. Girvin, Circuit QED: Superconducting qubits coupled to microwave photons, in *Quantum Machines: Measurement and Control of Engineered Quantum Systems* (Oxford University Press, Oxford, 2014), pp. 113–256.
- [54] L. S. Schulman, *Phys. Rev. A* **57**, 1509 (1998).
- [55] D. A. Lidar (2019), [arXiv:1902.00967](https://arxiv.org/abs/1902.00967).
- [56] J. M. Gambetta, A. Blais, D. I. Schuster, A. Wallraff, L. Frunzio, J. Majer, M. H. Devoret, S. M. Girvin, and R. J. Schoelkopf, *Phys. Rev. A* **74**, 042318 (2006).
- [57] T. Thorbeck, A. Eddins, I. Lauer, D. T. McClure, and M. Carroll, *PRX Quantum* **4**, 020356 (2023).
- [58] Q. Ai, D. Xu, S. Yi, A. G. Kofman, C. Sun, and F. Nori, *Sci. Rep.* **3**, 1752 (2013).
- [59] G. A. Álvarez, D. D. Bhaktavatsala Rao, L. Frydman, and G. Kurizki, *Phys. Rev. Lett.* **105**, 160401 (2010).
- [60] X. Cao, Q. Ai, C.-P. Sun, and F. Nori, *Phys. Lett. A* **376**, 349 (2012).
- [61] A. Auffèves, D. Gerace, J.-M. Gérard, M. F. Santos, L. C. Andreani, and J.-P. Poizat, *Phys. Rev. B* **81**, 245419 (2010).